Scandinavian Journal of Metallurgy 15 (1986) 97–103

An Analysis of Cooling Curves from the Fusion Zone of Steel Weld Deposits

*L.- E. Svensson, B. Gretoft and H.K.D.H. Bhadeshia**

ESAB AB, Gothenburg, Sweden
* University of Cambridge, Department of Metallurgy and Materials Science, Cambridge CB2 3QZ, U.K.

Experimentally determined cooling curves for the fusion zone of manual metal arc and submerged arc welds have been rationalised in terms of a theory for three-dimensional heat flow. The cooling curves were obtained for a wide range of welding conditions in which the welding current, voltage, speed and interpass temperature were varied, with the joint geometry being fixed to ISO-2560, the standard geometry for all-weld-metal tests. With the help of a recent model for the prediction of microstructure in weld deposits, the heat-flow analysis is used in understanding the effect of heat input on the microstructure of low-alloy steel weld deposits. It is demonstrated that the results can be used to predict trends in microstructure as a function of heat input, by analysing a large amount of published data on weld deposits.

Introduction

The way in which a weld deposit cools from the liquid state is known to have profound effects on its subsequent properties, homogeneity, microstructure and state of residual stress (see [1–6]). There is now a model [5] capable of estimating quantitatively the microstructure of the fusion zone of low-alloy steel welds deposited by arc welding techniques, as a function of the chemical composition. The austenite grain structure and the cooling curve of the fusion zone have, however, to be measured experimentally in each case. This clearly limits the usefulness of the model, the original aim of which was to enable the theoretical design of welding consumables and procedures.

For many applications, an approximate knowledge of the cooling time between specified temperatures is a sufficient characterisation of the cooling conditions of the weld deposit. On the other hand, a calculation of the microstructure requires a detailed knowledge of the cooling rate at any temperature where the austenite to ferrite transformation becomes thermodynamically possible [5].

In this paper, we attempt to rationalise cooling curves obtained from the fusion zones of arc welds. There is no reliable method for calculating such cooling curves as a function of welding current, voltage, speed, interpass temperature, arc transfer efficiency and joint geometry. This is not surprising since the deposition process is by nature turbulent, with heat transfer between the arc plasma, flux, base metal and the molten deposit itself. For manual metal arc welds, there must additionally exist random fluctuations due to human error. Bearing these difficulties in mind, our aim was to try and represent quantitatively the major variables controlling the cooling behaviour of arc welds of a given joint geometry, and to use these results in relating heat input to microstructure.

Experimental

The welds were deposited using the manual metal arc and submerged arc welding techniques, the joint geometry being compatible with ISO-2560; such joints are commonly used in the development of electrodes. The welding was carried out in the flat position using a stringer bead technique, the parent plate thickness being 20 mm. The plate length used was 330 mm and 550 mm for manual metal arc and submerged arc welds respectively, the half width of the plate being 150 mm in each case. 4 mm diameter electrodes (proprietary designation ESAB OK 48.00) were used for manual metal arc welding, and a medium manganese 4 mm diameter wire (OK Autrod 12.22) combined with an aluminate basic flux (OK Flux 10.71) was used for the submerged arc welds. The welding current, voltage and interpass temperature were systematically varied to cover a range typical of normal applications. The actual conditions used are presented in Table I, which also contains other data to be discussed later.

Weld cooling curves were obtained by harpooning Pt/Pt-13 Rh wt. % thermocouples at an angle of about 45° to the vertical, into the centre of the weld deposit, immediately after the passage of the welding arc. The cooling curves were recorded on a Philips PM9832 chart recorder. Interpass temperatures were monitored using temperature crayons and thermocouple probes placed on the weld surface.

Results and discussion

The nature of heat flow during welding can be two-dimensional, three-dimensional or somewhere in between these extremes, depending on the energy input and effective

Table I: *Details of welding conditions used to deposit manual metal arc (MMA) and submerged arc (SA) welds. I, V, S and T_i represent the welding current (Amps), voltage (V), welding speed (mm/s) and interpass temperature (°C) respectively. The constants C_1 and C_2 are derived using Eq. (1b), with the units of Q being J/m. Δt is the time (seconds) taken to cool from 800 → 500 °C. R is the linear correlation coefficient representing the fit of the experimental data to Eq. (1b).*

Weld	I	V	T_i	S	C_1	C_2	R	Δt	Bead
MMA1	180	24	25	1.2	3.4	2.480	0.998	31.2	
MMA2	180	24	100	1.2	223.3	1.833	0.985	38.0	
MMA3	180	24	200	1.2	50.0	2.064	0.997	63.3	
MMA4	179	24	250	1.2	5.9	2.417	0.969	89.3	
MMA5	166	23	25	1.7	20.4	2.293	0.997	10.7	
MMA6	167	23	100	1.7	435.7	1.770	0.990	18.1	
MMA7	167	23	250	1.7	18081.0	1.201	0.991	23.3	
MMA8	167	23	25	3.4	228.4	1.889	0.995	6.3	
MMA9	167	22	100	3.7	3574.0	1.461	0.990	6.7	
MMA10	167	23	200	3.5	200.6	1.878	0.993	14.7	
MMA11	180	24	250	3.6	2316.7	1.515	0.995	15.1	
MMA12	180	24	250	3.6	472.4	1.742	0.995	19.5	
MMA13	180	23	240	4.0	1191.1	1.695	0.998	8.4	
MMA14	190	23	250	4.0	1795.7	1.632	0.995	8.9	*
SA1	450	30	250	6.7	2657.4	1.609	0.988	15.6	3
SA2	450	30	250	6.7	1967.0	1.637	0.980	17.9	7
SA3	550	30	250	6.7	2842.3	1.647	0.996	14.3	4
SA4	550	30	250	6.7	603.0	1.784	0.972	30.1	8
SA5	550	30	250	6.7	2337.0	1.640	0.974	18.1	11
SA6	650	30	250	6.7	330.9	2.003	0.990	17.9	5
SA7	650	30	250	6.7	392.9	1.884	0.974	30.3	9
SA8	650	30	250	6.7	1445.0	1.616	0.991	39.8	13
SA9	650	30	250	7.0	29894.1	1.188	0.959	23.0	
SA10	580	29	175	9.2	11141.8	1.392	0.992	9.3	6
SA11	580	29	175	9.2	4470.2	1.498	0.986	12.2	10
SA12	580	29	175	9.2	275.7	1.937	0.980	13.6	14
SA13	500	30	250	7.0	16079.0	1.304	0.986	16.6	

* data from [5].

plate thickness [7–10]. For welds of the geometry used in the present study, cooling curves are best represented in terms of the theory of three-dimensional heat flow [5]. The magnitude of the cooling rate, (dT/dt), is then approximately given by [7]:

$$dT/dt = 2\pi k(T-T_i)^2/(Q\eta) \quad (1a)$$

where k is the thermal conductivity of solid iron, Q is the electrical energy input per unit length of weld deposit and η is the arc energy transfer efficiency, taken to be 0.775 for manual metal arc welds and 0.95 for submerged arc welds [1]. For three-dimensional heat flow and at temperatures well below the melting point, the cooling rate in the fusion zone is virtually independent of position [7].

Eq. (1a) has been found to be inadequate in representing experimental cooling curves [5]. Other heat flow models (such as that of Rosenthal [10]) were also found [5] unsuitable for application to the fusion zone. If Eq. (1a) is rewritten as

$$dT/dt = (C_1/Q\eta)\,(T-T_i)^{C_2} \quad (1b)$$

and if C_1 and C_2 are taken to be adjustable constants, then it accurately represents cooling conditions over the temperature range 800–500 °C [5]. The time Δt taken for the weld to cool between 800 and 500 °C can be calculated by integrating Eq. (1b):

$$\Delta t = [Q\eta/(C_1(1-C_2))]\,[(T-T_i)^{(1-C_2)}]\,\begin{matrix}800\\500\end{matrix} \quad (1c)$$

The experimental cooling curves were analysed using Eq. (1b), and the values of C_1 and C_2 together with the correlation coefficients (R) describing the fit with Eq. (1b) are given in Table I (the units of Q in Eq. (1b) are in J/m). Eq. (1b) is an excellent representation of individual cooling curves, although the values of C_1 and C_2 vary widely between different experiments; large values of C_1 lead to small corresponding values of C_2 and this makes Eq. (1b) sensitive to variations in cooling rates. From the point of view of obtaining a general equation for describing the cooling curve, this approach is unsatisfactory since different constants apply in each case. A better method would be to put all the experimental data together (rather than analyse individual curves) and then apply Eq. (1b) to the entire set of data; results using all the data are summarised in Table II.

Table II shows that Eq. (1b) can be used to approximate the cooling curve data, especially if the manual metal arc and submerged arc welds are dealt with separately. The actual experimental data are illustrated in Fig. 1. The level of prediction seems reasonable in view of the complications involved in considering heat flow in the fusion zone. Some of the scatter illustrated in Fig. 1 arises because in welding technology, the interpass temperature does not imply that the whole assembly being welded is at T_i, but that the weld

Table II. *Analysis of all experimental data. The first standard error (SE) is for the regression constant ($\ln[C_1]$) in a plot of $\ln[(dT/dt)Q\eta]$ versus $\ln[T-T_i]$; R represents the correlation coefficient for the plot. The second standard error is for the regression coefficient C_2.*

	C_1	SE	C_2	SE	R
All data of Table I	3381.2	0.525	1.491	0.086	0.816
MMA data of Table I	1324.8	0.511	1.600	0.083	0.900
SA data of Table I	4359.0	0.524	1.510	0.087	0.911

is at a temperature T_i before the next bead is deposited; the parent plate remote from the weld (say at a distance x) need not be at T_i and is usually at a temperature $T_o < T_i$. As welding proceeds, the gradient $[(T_i-T_o)/x]$ decreases with the bead number in multipass welds. Consequently, the heat flux away from the weld reduces even though the welding conditions (I, V, S, T_i) are kept constant, since the diffusion of heat varies directly with this gradient. This effect was observed experimentally in submerged arc welds, where repeat experiments showed that Δt increases with bead number for constant I, V, S and T_i (Table I).

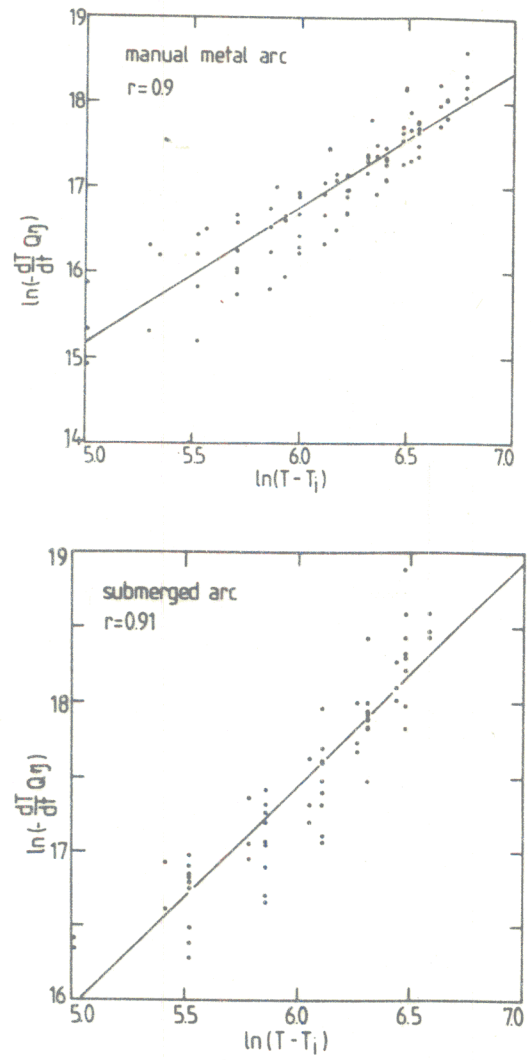

Fig. 1. *Plots of $\ln\{(dT/dt)Q\eta\}$ versus $\ln\{T-T_i\}$, showing the fit of the entire data set for a particular welding process, with Eq. (1b). a) Manual metal arch weld data; b) submerged arch weld data.*

Effect of heat input on microstructure

Analysis of published data

Having established an approximate method of relating the cooling curve to welding parameters, it should be possible to analyse published experimental data on the influence of heat input on the microstructure of low-alloy steel weld deposits, using the model developed by Bhadeshia *et al.*[5]

The microstructure of welds is complex, consisting of allotriomorphic ferrite (α) which grows diffusionally at austenite (γ) grain boundaries, Widmanstätten ferrite (α_w) which nucleates at α/γ boundaries and grows by a displacive mechanism in the form of thin wedge shaped plates at a rate controlled approximately by the diffusion of carbon in the austenite ahead of the interface, acicular ferrite (α_a) which nucleates intragranularly at inclusions but whose detailed transformation mechanism is not clear, and finally, microphases consisting of mixtures of martensite, degenerate pearlite and retained austenite, all formed from the residual austenite remaining untransformed after α, α_w and α_a have formed.

Implications of using approximate cooling curves

The method of computing the microstructure has been described in detail in [5] and will be summarised later; it is instructive to examine first the implications of using the coefficients of Table II, rather than the measured cooling curve, on the accuracy of microstructure prediction. Fig. 2 illustrates the effect of using the coefficients of Table II on the calculated microstructure, as compared with calculations based on the measured cooling curve. Agreement between the measured microstructure and that calculated is best when the measured cooling curve is used; the heat flow parameters given in Table II can nevertheless be used in estimating the trends in microstructure when the exact cooling curves are not known.

The evolution of microstructure must depend on cooling

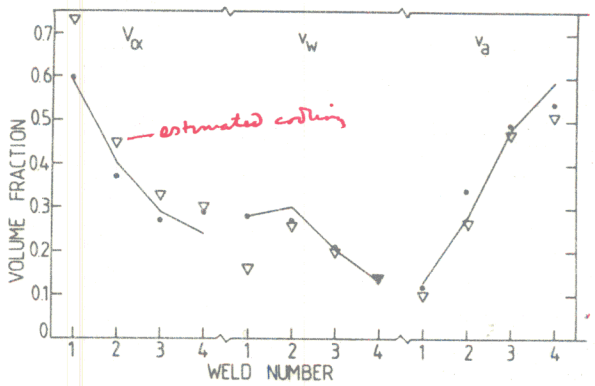

Fig. 2. *An illustration of the influence of using the heat flow parameters given in Table II, on the calculated microstructure of four low-alloy steel, manual metal arc weld deposits. The welds, in an order which gives a decreasing amount of allotriomorphic ferrite, have the compositions Fe-0.029C-0.55Si-1.08Mn, Fe-0.061C-0.53Si-1.01Mn, Fe-0.080C-0.58Si-1.15Mn and Fe-0.100C-0.55Si-1.02Mn respectively. The lines represent the actual microstructure, as measured by Bhadeshia et al. [5], the dots represent the microstructure as calculated using the measured cooling curve [5], and the triangles represent the microstructure calculated using the MMA parameters quoted in Table II. The microstructure calculations are all carried out according to the model presented in [5].*

Table III. *Data on austenite grain width (taken to be equivalent to $\bar{L}_{tn}$) as a function of C, Mn, Si and Q (after Evans [13–15].*

$\bar{L}_{tn}$ μm	C wt.%	Si wt.%	Mn wt.%	Q kJ/mm
84	0.055	0.35	1.93	0.6
93	0.051	0.32	1.80	1.0
100	0.045	0.26	1.69	2.2
134	0.047	0.25	1.73	4.3
105	0.045	0.30	0.65	1.0
102	0.044	0.32	0.98	1.0
99	0.044	0.32	1.32	1.0
94	0.045	0.30	1.72	1.0
94	0.059	0.33	0.60	1.0
92	0.063	0.35	1.00	1.0
86	0.066	0.37	1.35	1.0
80	0.070	0.33	1.77	1.0
73	0.099	0.35	0.65	1.0
69	0.098	0.32	1.05	1.0
66	0.096	0.30	1.29	1.0
63	0.093	0.33	1.65	1.0
67	0.147	0.40	0.63	1.0
63	0.152	0.41	1.00	1.0
62	0.148	0.38	1.40	1.0
62	0.141	0.36	1.76	1.0
74	0.050	0.26	1.73	0.7
82	0.059	0.32	1.80	1.1
93	0.052	0.29	1.73	1.5
100	0.054	0.27	1.62	1.8

rate since the nucleation and growth rates vary with temperature; there is however, an additional effect due to the dependence of the austenite grain size (which has a major effect on microstructure) on heat input, an effect which has not been quantitatively characterised previously. The alloy composition also influences the γ grain size** and the following analysis was carried out to quantitatively express these relationships.

The austenite grain size of Fe-C-Si-Mn MMA welds

In low-carbon steel welds, solidification begins with the epitaxial nucleation and cellular growth of δ-ferrite from the melt. The columnar γ grains then evolve by the transformation of δ-ferrite. The morphology of the resulting γ grains can approximately be described as consisting of space-filling hexagonal prisms of length 'c' and cross section side-length 'a' [5, 11]. It turns out that because $c \gg a$, only the parameter a needs to be measured or predicted in order to calculate the microstructure.

Weld deposits are usually examined in transverse section (on a plane normal to the welding direction) and in this section, the γ grains have an anisotropic, columnar shape. It is usual to express the "size" of the grains in terms of a "grain width" which really is a measurement of a mean lineal intercept ($\bar{L}_{tn}$) determined by superimposing test lines on a *t*ransverse section, not in a random orientation relative to the microstructure but in a direction *n*ormal to the major axes of the grain sections. In these circumstances, the test lines should all approximately be parallel to the basal planes of the hexagonal prisms and it has been shown that [11, 12]:

$$\bar{L}_{tn} = \pi a \cos\{30°\}/2 \quad (3)$$

Evans [13–15] has published several measurements (Table III) of austenite grain widths for Fe-C-Si-Mn manual metal arc welds deposited using a variety of welding conditions and electrode compositions for a weld geometry consistent with ISO 2560. A multiple regression analysis of the grain width (taken to be equivalent to $\bar{L}_{tn}$) versus C, Si, Mn and Q gave the following relation for the range of compositions given in Table III:

$$\bar{L}_{tn}\,(\mu m) = 64.5 - 445.8(\text{wt.\% C}) + 138.6(\text{wt.\% Si}) - 7.591(\text{wt.\% Mn}) + 16(\text{Q, kJ/mm}) \quad (4)$$

The level of agreement between experimental data and Eq. (4) is illustrated in Fig. 3, the multiple correlation coefficient for the plot being 0.97. Evans does not quote the oxygen or inclusion content (these two quantities are directly related [16]) of the welds, but the high value of the correlation coefficient indicates that any effect due to inclusions must be small.

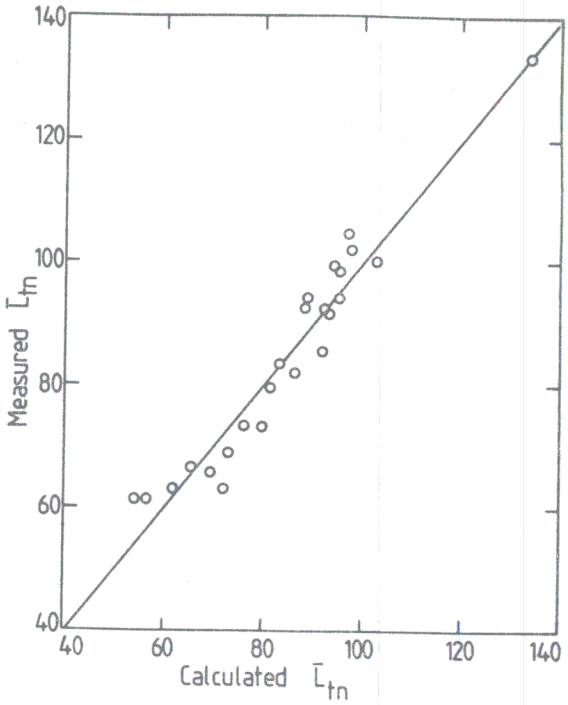

Fig. 3. *Plot of calculated austenite grain width (Eq. (4)) versus measured widths as reported by Evans [13–15].*

Further analysis of published data on the relationship between microstructure and heat input

Evans has published quantitative data on the influence of heat input on the microstructure of low-alloy steel weld deposits. The data are presented in Table IV. It should be possible to predict the microstructural variations listed in Table IV using the model developed by Bhadeshia *et al.* [5]. The model has been tested successfully for Fe-Si-Mn-C al-

** Inclusions in welds have been suggested [17, 18] to limit the size of austenite grains in weld deposits, but recent work [5, 11] shows this is not the case since the driving force for γ boundary motion during the δ to γ transformation increases indefinitely with undercooling so that boundary pinning by inclusions is ineffective.

Table IV. *Quantitative data on the variation of microstructure with heat input and chemical compositition (after Evans [13]). The data are for manual metal arc welds (ISO 2560, welded in the flat position using DC + and with $T_i = 200°$. The microphase content, which should be very small, is implicitly included in the acricular ferrite and Widmanstätten ferrite volume fractions.*

No.	C wt.%	Si wt.%	Mn wt.%	Q kJ/mm	v_α	v_w	v_a
1	0.044	0.32	0.62	0.6	0.56	0.13	0.31
2	0.046	0.31	0.96	0.6	0.38	0.11	0.51
3	0.050	0.38	1.42	0.6	0.26	0.05	0.69
4	0.055	0.35	1.93	0.6	0.19	0.04	0.77
5	0.037	0.29	0.60	1.0	0.60	0.14	0.26
6	0.039	0.29	0.94	1.0	0.40	0.11	0.49
7	0.048	0.35	1.41	1.0	0.30	0.06	0.64
8	0.051	0.32	1.80	1.0	0.21	0.06	0.73
9	0.038	0.24	0.55	2.2	0.64	0.13	0.23
10	0.036	0.24	0.89	2.2	0.41	0.11	0.48
11	0.042	0.28	1.37	2.2	0.34	0.06	0.60
12	0.045	0.26	1.69	2.2	0.25	0.06	0.69
13	0.043	0.20	0.52	4.3	0.67	0.16	0.17
14	0.042	0.20	0.93	4.3	0.45	0.15	0.40
15	0.043	0.24	1.37	4.3	0.37	0.06	0.57
16	0.047	0.25	1.73	4.3	0.27	0.06	0.67

loys and for Fe-Si-Mn-Ni-C welds and the method is illustrated in Fig. 4a.

The model requires an input of chemical composition (from Table IV), the austenite grain parameter 'a' (previously measured, but in the present work calculated using Eq. (3) and Eq. (4)) and and the cooling curve of the weld deposit, over the range 800 → 500 °C. In the absence of an experimentally determined cooling curve, Eq. (1b) and the data of Table II can be used to provide calculated cooling rates. As can be seen from Table IV, Evans used 0.6, 1.0, 2.2 and 4.3 kJ/mm heat input to produce the manual metal arc welds and reported corresponding Δt measurements (for the range 800–500 °C) as 4, 7, 13 and 34 s respectively. These data are well represented by Eq. (1a) if $C_2 = 1.60$ (Table II), but taking C_1 to be 1324.8 (Table II) overestimated Δt (7, 11, 24, 47 s) values so that C_1 was set equal to 2155.0, giving good agreement with Evan's reported Δt values (4, 7, 15, 29 s).

Having established the input data, the next step involves the calculation of multicomponent phase diagrams (Fig. 4a), time-temperature-transformation (TTT) and continuous-cooling transformation (CCT) diagrams, which when combined with the cooling rate equation gives the various reaction-start and finish temperatures. The calculated phase diagrams, TTT and CCT curves and transformation temperatures are not included in this paper for space considerations. The volume fraction of allotriomorphic ferrite can be predicted by assuming the paraequilibrium thickening of layers of ferrite [5], and is given by:

$$V_\alpha = 2.04[4qC_3(a-qC_3)/a^2)] + 0.035 \quad (5a)$$

where $C_3 = \tan(30°)$.

Widmanstätten ferrite is the next phase to grow on further cooling and its volume fraction v_w is given by:

$$v_w = 3.34G(a-2qC_3)t_2^2/a^2 \quad (5b)$$

where G is the α_w growth rate and t_2 is the time during which α_w forms. The time interval t_3 required for an α_w plate to grow across a partially transformed γ grain is given by:

$$t_3 = 2(a\sin(60°) - q)/G \quad (5c)$$

To account for physical impingement between α_w and α_a, a further time interval t_c is defined; if $t_3 < t_c$, α_w growth occurs essentially without impingement and $t_2 = t_3$. If on the other hand $t_3 > t_c$, then $t_2 = t_c$, irrespective of the amount of austenite remaining untransformed. t_c can at the moment only be determined by fitting eqs. 5a–c to data from just one weld; using the data of weld 1 (Table IV), t_c was

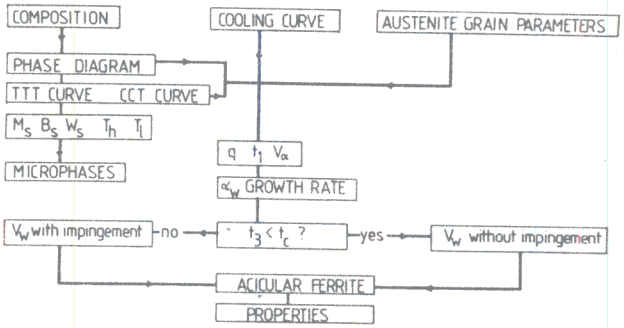

Fig. 4a. *Flow chart illustrating the steps involved in the calculation of the microstructure. M_s, B_s, W_s are the thermodynamically calculated martensite, bainite and Widmanstätten ferrite start temperatures respectively, T_h and T_l are the temperatures at which allotriomorphic ferrite formation begins and ends respectively, q is the half-thickness of the α layer at the γ grain boundaries, t_1 is the time available for α growth, t_3 is the time required for an α_w plate to grow across a γ grain, t_c is the maximum time available for unrestricted α_w growth prior to hard-impingement with intragranularly nucleated α_a. V_α, v_w, v_a and v_m represent the volume fractions of α, α_w, α_a and microphases respectively.*

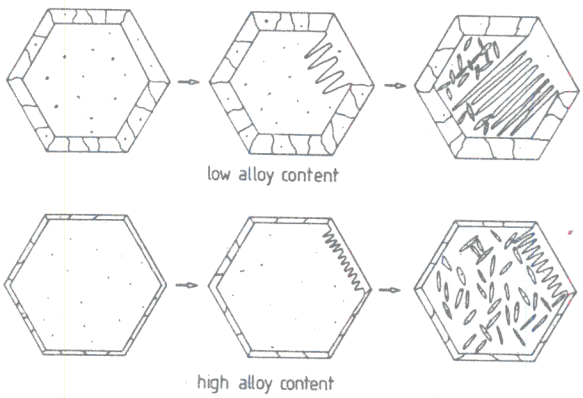

Fig. 4b. *Schematic diagram illustrating the development of microstructure in weld deposits. The hexagons represent cross-sections of columnar γ grains whose boundaries first become decorated with a uniform layer of polycrystalline α (illustrated thickness = q) and α_w growth follows later. Depending on it growth rate G, α_w then impinges with α on the opposite boundary (low-alloy content), or with α_a nucleated on inclusions (black dots) in the case of high-alloy deposits. The digram takes no account of the influence of alloy content on 'a'.*

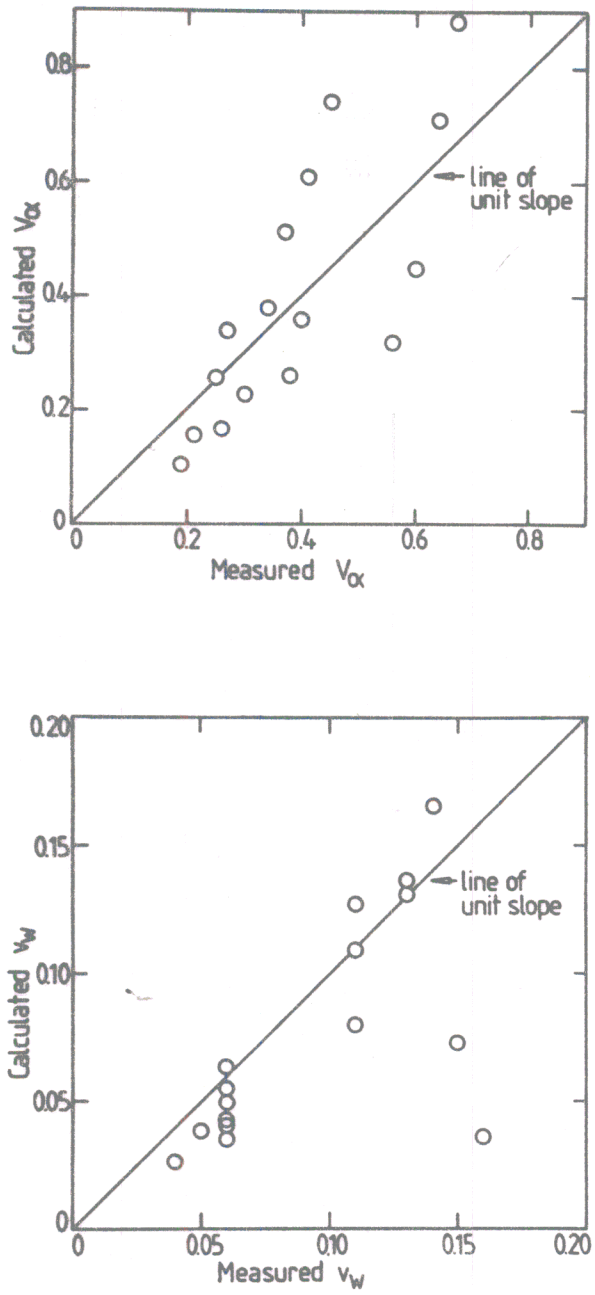

Fig. 5. *Plots of the calculated volume fractions of (a) allotriomorphic ferrite and (b) Widmanstätten ferrite, versus the experimental measurements of Evans [13], for the welds listed in Table IV.*

found to be 0.095 s, and it is this value which is used in the subsequent analysis of all other welds.

In Evan's measurements, the volume fraction v_a of acicular ferrite is given by $v_a = 1 - v_w - V_\alpha$ so that any microphases are implicitly included in the v_a and v_w measurements. Since the volume fraction of microphases in such welds are usually small ($\sim< 0.05$), this approximation is reasonable and is also used in the present calculations.

Fig. 5a shows that the calculated V_α values are in reasonable agreement with those measured. Fig. 5b shows that the measured v_w values are also in reasonable agreement with those calculated; the two values which depart most from experimental measurements are from welds with exceptionally high values of V_α, when small errors in the latter lead to relatively large errors in v_w since v_w values are small in the present alloys.

Conclusions

Experimentally determined cooling curves for manual metal arc and submerged arc welds of a particular geometry have been rationalised in terms of a simple three-dimensional heat flow equation which represents the cooling rate (over the temperature range 800 → 500 °C) as a function of welding current, welding voltage, deposition speed and interpass temperature; the cooling rate is assumed to be independent of the position within the fusion zone of a given bead. Individual cooling curves accurately (correlation > 0.95) follow the form of the cooling rate equation, but the certain parameters (C_1, C_2) within the equation vary in each case. However, if all the cooling curves from a particular welding process are analysed together, then the level of agreement between theory and experiment decreases somewhat (correlation 0.9), but the cooling curves can all be rationalised by just two constants. The latter approach has to be adopted for microstructure modelling in cases where experimentally measured cooling curves are not available; this should inevitably lead to errors in the absolute levels of calculated quantities, but trends in microstructure can nevertheless be predicted.

Published experimental data on the variation of microstructure with heat input have been analysed using the heat flow equation and a model for the development of microstructure in low-alloy steel weld deposits. The results are on the whole in good agreement with theory. The austenite grain size can empirically be expressed as a function of the alloy composition and heat input to a high degree of accuracy, without taking any account of the presence of inclusions.

Acknowledgements

The authors are grateful to ESAB AB (Sweden) for financial support and for the provision of laboratory facilities, and to Professor D. Hull for the provision of laboratory facilities at the University of Cambridge.

References

1. Easterling, K.E., *Introduction to the Physical Metallurgy of Welding,* Butterworths, London, p. 71 (1983).
2. Barlow, J.A. and Percival, D.F., An initial study of thermal cycle prediction in submerged arc welds. *Welding Institute Research Report* 218 (1983), Abington, Cambridge.
3. Davey, T.G., The effect of plate size on the submerged arc weld thermal cycle. *Welding Institute Research Report* 156 (1981), Abington, Cambridge.
4. Boulton, N.S. and Lance Martin, H.E., Residual stresses in arc welded plates. Proc. of the Institution of Mechanical Engineers, London, 133 (1936) 295–339.
5. Bhadeshia, H.K.D.H., Svensson, L.-E., and Gretoft, B., A model for the development of microstructure in low-alloy steel (Fe-Mn-Si-C) weld deposits. *Acta Metall.,* 33 (1985) 1271–1283.
6. Fredriksson, H., and Stjerndahl, J., Solidification of iron-base alloys. *Metal Science,* 16 (1982) 575–585.
7. Weisman, C., Editor, *Welding Handbook,* 7th edition, Vol. 1, p. 79, American Welding Society, Florida (1981).
8. Adams Jr., C.M., Cooling rates and peak temperatures in fusion welding. *Welding Journal,* 35 (1958) 210–215.

9. Jhaveri, P., Moffatt, W.G., and Adams Jr., C.M., The effect of plate thickness and radiation on heat flow in welding and cutting. *Welding Journal,* 41 (1962) 12s–16s.
10. Rosenthal, D., The theory of moving sources of heat and its application to metal treatment. *Transactions ASME,* 68 (1946) 819–866.
11. Bhadeshia, H.K.D.H., Svensson L.-E., and Gretoft, B., The austenite grain structure of low-alloy steel weld deposits. Submitted to the *Journal of Materials Science,* 1985.
12. Gretoft, B., Bhadeshia, H.K.D.H., and Svensson, L.-E., Development of microstructure in the fusion zone of steel weld deposits. *Acta Stereologica,* in press, 1985.
13. Evans, G.M., The effect of carbon on the microstructure and properties of C-Mn all-weld metal deposits. International Welding Institute Doc. II-A-546-81, 1981.
14. Evans, G.M., Effect of heat-input of the microstructure and properties of C-Mn all-weld metal deposits. International Welding Institute Doc. II-A-490-79, 1979.
15. Evans, G.M., Effect of electrode diameter on the microstructure and properties of C-Mn all-weld metal deposits. International Welding Institute Doc. II-A-469-79, 1979.
16. Widgery, D.J., Factors controlling fracture by microvoid coalescence in as-deposited weld metals. Welding Institute Research Members Seminar on the Toughness of Weld Metals, Newcastle-upon-Tyne, 1977.
17. Harrison, P.L., and Farrar, R.A., Influence of oxygen-rich inclusions on the $\gamma \rightarrow \alpha$ transformation in high-strength low-alloy steel weld metals. *J. Mat. Sci.,* 16 (1981) 2218.
18. Cochrane, R.C. and Kirkwood, P.R., Trends in Steels and Consumables for Welding. Proc. of the Welding Institute Conference, London, (1978) p. 103.

Received November 22, 1985